Emergence of quantum spin frustration in spin-1/2 Ising-Heisenberg model on a decorated honeycomb lattice

Onofre Rojas
Department of Physics, Institute of Natural Science, Federal University of Lavras, 37200-900, Lavras-MG, Brazil

(Received 3 March 2022; accepted 28 June 2022; published 11 July 2022)

We study the spin-1/2 Ising-*XXZ* model on a decorated honeycomb lattice composed of five spins per unit cell, one Ising spin, and four Heisenberg spins. This model involving the Heisenberg exchange interaction is one of the few models that can be exactly solvable through the generalized star-triangle transformation. The significance of this model is its close relationship to the fully decorated quantum Heisenberg honeycomb lattice since 4/5 of the particles are Heisenberg spins. We investigate the phase diagram at zero temperature and identify a relevant quantum spin frustrated phase resulting from the contribution of quantum Heisenberg exchange interaction. We obtain an exact residual entropy for the quantum spin frustrated phase, which coincides with the residual entropy of the antiferromagnetic spin-1/2 Ising model on a triangular lattice. We also thoroughly explore its thermodynamic properties, focusing mainly on the frustrated region such as entropy, specific heat, spontaneous magnetization, and critical temperature under several conditions.

DOI: 10.1103/PhysRevE.106.014109

I. INTRODUCTION

One of the topics of intense research in statistical physics is frustrated spin systems, showing numerous fascinating phenomena. For example, the role of frustration in the emergence of magnetic phases and the nature of phase transitions received a great deal of attention in the last decades. In this context, lattices of quantum spin models are relevant, like the Heisenberg model that describes in detail several synthesized compounds. Typically, spin models in statistical physics cannot be solved exactly, so most of them can only be studied numerically. Therefore, the exact solutions were only achieved in limited cases. However, after the solution found by Onsager for the two-dimensional (2D) Ising model [1], inspired several attempts to solve other similar models. Such as the honeycomb lattice [2–4], whose exact solution of a honeycomb lattice with an external magnetic field was provided by Wu [5]. Besides, kagomé lattice was also widely discussed in the literature [6,7] and reference therein.

One of the candidates for obtaining spintronic devices with high performance and high integration density may be 2D semimetallic materials, thus becoming highly desirable. Based on first-principles calculations, was predicted a potential candidate of 2D half-metals, named monolayer Mg_3Si_2 [8], which has a honeycomb-kagomé lattice pattern. Also proposed was a 2D-silicon semiconductor by introducing kagomé topology into a honeycomb lattice, i.e., a hybrid honeycomb-kagomé(hhk) structure [9], which demonstrates high geometric stability and excellent semiconducting properties of the hhk-silicene. Other theoretical investigations on honeycomb-kagomé lattice appear in a variety of compounds, such as 2D honeycomb-kagomé Be_3Pb_2 [10]. This compound exhibits a nontrivial topology in the electronic structure that accompanies the spin-orbit coupling (SOC) induced by the energy gap bandwidth. Recently, several other investigations have been developed, with a number of exotic properties [11–14].

Normally, geometric frustration occurs within a triangular spin structures. When the antiferromagnetic exchange interactions cannot be satisfied simultaneously, we achieve a considerable degenerated ground state that leads to a frustration. In such a way, frustrated magnets have been attracted great scientific interest because of quantum spin liquid in 2D systems, which has been pointed to play a striking role in high-temperature superconductors. In this sense, there are several investigations concerning geometrically frustrated kagomé lattice compounds, which are challenging topics. Some materials with spin-1/2 kagomé structures present the liquid state of quantum spin at zero temperature, such as the antiferromagnetic kagomé lattice. Like atacamite family [15] whose general formula is $Zn_xCu_{4-x}(OH)_6Cl_2$ with $(0 \leqslant x \leqslant 1)$, which follows a regular kagomé lattice structure. Using the single-crystal samples of the antiferromagnet spin-1/2 kagomé-lattice [16] $ZnCu_3(OD)_6Cl_2$ (also called herbertsmithite), certain relevant features of the quantum spin liquid phase were observed.

Several decorated spin models can be solved by applying the well-known decoration transformation introduced in the 1950s by Fisher [17] and Syozi [18]. Later generalized for arbitrary spins, such as the classical or quantum spin models [19–21]. This transformation is essential because we can map cumbersome models into simple or exactly solvable models. In what follows, we mention a few typical examples of this approach: the geometrical frustrated Cairo pentagonal lattice Ising model [22], the geometrically frustrated Ising-*XXZ* spin on expanded kagomé lattice [23], the *XXZ*-Ising model on the triangular kagomé lattice with spin-1/2 [24,25], and mixed-spin Ising model on a honeycomb lattice [26]. Furthermore,

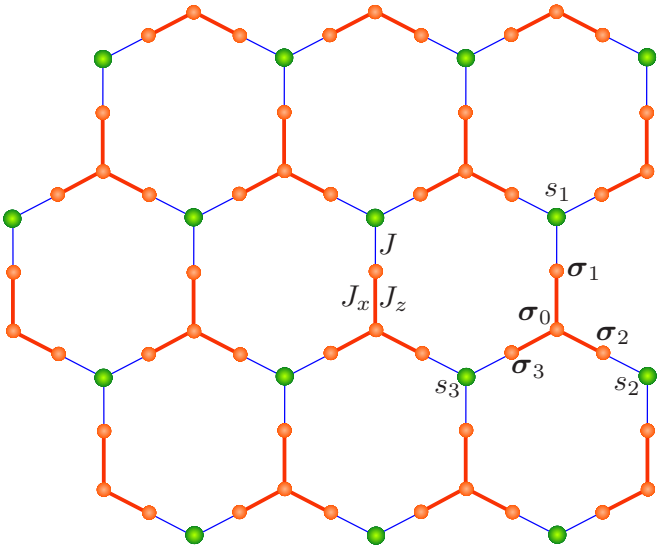

FIG. 1. Spin-1/2 Ising-Heisenberg decorated honeycomb lattice, orange spheres correspond to Heisenberg spins, and green spheres denote Ising spins. Orange lines correspond to Heisenberg exchange interactions, and blue lines indicate the Ising exchange interactions.

2D square-hexagon (denoted for simplicity by 4–6) *XXZ*-Ising with the spin-1/2 model was investigated using the same approach [27]. Similarly, two-dimensional 3–12 lattice is also known in the literature [28,29] as the star lattice, Fisher lattice, expanded kagomé lattice, or even triangular honeycomb lattice. The study of these models was based on their close relationship with geometrically frustrated magnetic polymers [30]. There are even several investigations concerning other Ising-Heisenberg lattices like bipyramidal plaquette [31,32], triangles-in-triangles lattices [33,34], martini lattice [35], and triangulated Husimi [36] and kagomé [37] lattices. It is also worth mentioning that there are investigations on spin-1/2 Heisenberg antiferromagnetic star lattice structure [38,39].

The outline of this report is as follows. In Sec. II, we present the spin-1/2 Ising-*XXZ* model on a decorated honeycomb lattice, so we map through the generalized star-triangle transformation technique into an effective triangular lattice. And subsequently, we investigate the ground-state phase diagram, showing an unconventional quantum spin frustration. Whereas, in Sec. III, we report the thermodynamics result for studying entropy, specific heat, critical temperature, and spontaneous magnetization. Finally, Sec. IV focuses on presenting our concussions.

II. ISING-*XXZ* MODEL ON A DECORATED HONEYCOMB LATTICE

A classical version of the spin-1/2 Ising model on a decorated honeycomb lattice has been considered by Syozi [18] and later Wu [5] investigated in the presence of an external magnetic field. However, before considering its fully quantum version, a natural generalization would be the spin-1/2 Ising-*XXZ* model on a decorated honeycomb lattice, as illustrated in Fig. 1, by Heisenberg spin (small sphere) and Ising spin (large sphere). Thus, the thick solid line between small spheres represents the exchange interactions of Heisenberg

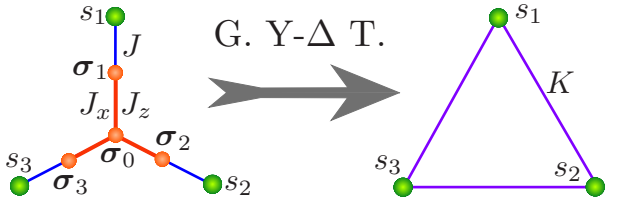

FIG. 2. Schematic representation of generalized star-triangle transformation (G. Y-Δ T.) of a spin-1/2 Ising-*XXZ* model of decorated three-leg star onto a spin-1/2 Ising model on a triangular structure.

spin, whereas the thin blue solid line bonds small and large spheres corresponding to Ising-type exchange interactions.

The Hamiltonian that describes the decorated honeycomb lattice (see Fig. 1), can be expressed as follows:

$$H = -\sum_{\langle i,j\rangle}\left[J_x\left(\sigma_i^x\sigma_j^x+\sigma_i^y\sigma_j^y\right)+J_z\sigma_i^z\sigma_j^z\right]-J\sum_{\langle i',l\rangle}\sigma_{i'}^z s_l, \quad (1)$$

where σ^α denotes the Heisenberg spin operator, with $\alpha = \{x, y, z\}$, and s_l denotes the Ising spin $s_l = \pm 1/2$. The first summation corresponds to the anisotropic Heisenberg exchange interaction between the nearest-neighbor spins, with J_x standing to the Heisenberg exchange interaction in xy component, and J_z corresponds to Heisenberg exchange interaction in the z component. The second summation indicates the Ising spin exchange interaction J between nearest Ising and Heisenberg spins.

A. Generalized star-triangle transformation

The model proposed in Eq. (1) could be viewed as a decorated Ising-*XXZ* model that can be mapped exactly by means of a generalized generalized star-triangle transformation [17–21], as illustrated in Fig. 2, which basically makes a partial trace over all Heisenberg spins, leaving only the Ising spins interaction between the nearest neighbors. Thus, we will consider a three-legged hybrid star system as schematically represented in Fig. 2 (left). The three internal bonds of the star are described by J_x and J_z corresponding to Heisenberg-type interactions, while the external legs are Ising-type interactions J, as shown in Fig. 2 (left). Hence, the Ising-*XXZ* model on decorated honeycomb lattice can be mapped onto a triangular lattice with effective Ising spin coupling K through a generalized star-triangle transformation approach [17–21], as displayed in Fig. 2 (right).

To carry out the lattice transformation, let us define the following operator:

$$\mathbf{V}(\{\boldsymbol{\sigma}, s\}) = e^{\beta\sum_{i=1}^{3}[J_x(\sigma_i^x\sigma_0^x+\sigma_i^y\sigma_0^y)+J_z\sigma_i^z\sigma_0^z+J\sigma_i^z s_i]}, \quad (2)$$

where $\{\boldsymbol{\sigma}, s\}$ denote $\{\boldsymbol{\sigma}_0, \boldsymbol{\sigma}_1, \boldsymbol{\sigma}_2, \boldsymbol{\sigma}_3, s_1, s_2, s_3\}$, and $\boldsymbol{\sigma} = \{\sigma^x, \sigma^y, \sigma^z\}$. The spin index s_l in Hamiltonian (1), was reindexed by s_i (same index of σ_i) just for simplicity, without imposing any restrictions. Thus, the Boltzmann factor of the decorated hybrid-spin model becomes

$$w(\{s\}) = \mathrm{tr}_{\{\sigma\}}[\mathbf{V}(\{\boldsymbol{\sigma}, s\})]. \quad (3)$$

The inner star system (decorated) is expressed as Heisenberg coupling, and it provides two configurations for Ising

TABLE I. Eigenvalues of spin-1/2 Heisenberg decorated triangles, in which the coefficients are given in Eqs. (4)–(8). The eigenvalues $\{\varepsilon_1^{(3)}, \varepsilon_2^{(3)}, \varepsilon_{14}^{(3)}, \varepsilon_{16}^{(3)}, \varepsilon_8^{(1)}\}$ are the originator of the ground-state energy of the spin-1/2 Ising-*XXZ* model in the decorated honeycomb lattice.

k	$\varepsilon_k^{(3)}$ for $\varsigma = 3/2$	$\varepsilon_k^{(1)}$ for $\varsigma = 1/2$
1	$-\frac{3}{4}(J_z + J)$	$-\frac{1}{4}(3J_z + J)$
2	$-\frac{3}{4}(J_z - J)$	$-\frac{1}{4}(3J_z - J)$
3	$-\frac{1}{4}(J_z + J)$	$-\frac{1}{4}(J_z + J)$
4	$-\frac{1}{4}(J_z + J)$	$-\frac{1}{4}(J_z + J)$
5	$-\frac{1}{4}(J_z - J)$	$\frac{1}{4}(J_z + \sqrt{J^2 + 4J_x^2})$
6	$-\frac{1}{4}(J_z - J)$	$\frac{1}{4}(J_z - \sqrt{J^2 + 4J_x^2})$
7	$\frac{1}{4}(J_z + \sqrt{J^2 + 4J_x^2})$	$\frac{1}{4}(J_z + \sqrt{B_+})$
8	$\frac{1}{4}(J_z + \sqrt{J^2 + 4J_x^2})$	$\frac{1}{4}(J_z - \sqrt{B_+})$
9	$\frac{1}{4}(J_z - \sqrt{J^2 + 4J_x^2})$	$\frac{1}{4}(J_z + \sqrt{B_-})$
10	$\frac{1}{4}(J_z - \sqrt{J^2 + 4J_x^2})$	$\frac{1}{4}(J_z - \sqrt{B_-})$
11	$\frac{1}{4}(J_z + \sqrt{J^2 + 16J_x^2})$	$2\sqrt{Q}\cos(\frac{\theta_+}{3}) - \frac{1}{12}(3J - J_z)$
12	$\frac{1}{4}(J_z - \sqrt{J^2 + 16J_x^2})$	$2\sqrt{Q}\cos(\frac{\theta_+ - 2\pi}{3}) - \frac{1}{12}(3J - J_z)$
13	$\frac{1}{4}(J_z - 2J + \sqrt{A_-})$	$2\sqrt{Q}\cos(\frac{\theta_+ - 4\pi}{3}) - \frac{1}{12}(3J - J_z)$
14	$\frac{1}{4}(J_z - 2J - \sqrt{A_-})$	$2\sqrt{Q}\cos(\frac{\theta_-}{3}) + \frac{1}{12}(3J + J_z)$
15	$\frac{1}{4}(J_z + 2J + \sqrt{A_+})$	$2\sqrt{Q}\cos(\frac{\theta_- - 2\pi}{3}) + \frac{1}{12}(3J + J_z)$
16	$\frac{1}{4}(J_z + 2J - \sqrt{A_+})$	$2\sqrt{Q}\cos(\frac{\theta_- - 4\pi}{3}) + \frac{1}{12}(3J + J_z)$

spins (legs); these correspond to the following configurations $\{+++\}$ and $\{++-\}$ (since the lattice is invariant under spin inversion). So by defining $\varsigma = s_1 + s_2 + s_3$, the pair configurations become $\varsigma = 3/2$ and $1/2$. A convenient way to obtain the trace over Heisenberg spin is diagonalizing the 16×16 matrix for both Ising spin configurations $\varsigma = 3/2$ and $\varsigma = 1/2$. In Table I is reported the 16 eigenvalues for both configurations. Some eigenvalues are large expressions, so we have denoted conveniently by using the following notations:

$$A_\pm = (J \pm 2J_z)^2 + 12J_x^2, \tag{4}$$

$$B_\pm = 5\left(2J_x^2 + J^2\right) \pm 2\sqrt{\left(2J^2 + 3J_x^2\right)^2 + 16J^2J_x^2}, \tag{5}$$

$$Q = \frac{1}{12}J^2 + \frac{1}{9}J_z^2 + \frac{1}{4}J_x^2, \tag{6}$$

$$R_\pm = \left(\frac{1}{8}J_z \mp \frac{1}{16}J\right)J_x^2 + \frac{1}{27}J_z^3 - \frac{1}{12}J^2J_z, \tag{7}$$

$$\theta_\pm = \arccos\left(\frac{R_\pm}{\sqrt{Q^3}}\right). \tag{8}$$

Indeed, the corresponding eigenvectors are also relevant, but we do not express them explicitly because they involve huge cumbersome algebraic expressions. Nevertheless, further on, we will use some of these eigenvectors mainly to study the quantum spin frustrated phase, and the thermal magnetization of the model.

Now we write the Boltzmann factor for the case $\varsigma = 3/2$, so for simplicity, we denote by $w(3/2) = w_3$,

$$w_3 = \sum_{k=1}^{16} e^{-\beta\varepsilon_k^{(3)}}, \tag{9}$$

where $\varepsilon_k^{(3)}$ means the eigenvalues of Heisenberg spins, which are given in Table I (second column).

Similarly, for $\varsigma = 1/2$, the Boltzmann factor becomes

$$w_1 = \sum_{k=1}^{16} e^{-\beta\varepsilon_k^{(1)}}, \tag{10}$$

and its eigenvalues $\varepsilon_k^{(1)}$ are given in Table I (third column).

However, let us assume that the Hamiltonian of spin-1/2 Ising model on the effective triangular lattice can be expressed as follows:

$$\mathcal{H}_{\text{eff}} = \tilde{\mathcal{H}} = -K_0 - K\sum_{\langle i,j\rangle} s_i s_j, \tag{11}$$

in which K_0 corresponds to an effective "constant" energy, and K is the effective coupling parameter of Ising model on the triangular lattice, while the summation is performed over the nearest-neighbor interactions. So, the Boltzmann factor per each unit cell is given by

$$\tilde{w}(\{s_1, s_2, s_3\}) = e^{\beta K_0 + \beta K(s_1s_2 + s_2s_3 + s_3s_1)}. \tag{12}$$

The spin-1/2 Ising model on the effective triangular lattice has only two configurations, $\{+++\}$ and $\{++-\}$ (or its spin inversion), corresponding to $\varsigma = 3/2$ and $\varsigma = 1/2$, respectively. Therefore, both models should be equivalent, and the Boltzmann factor for both lattices must satisfy the condition $\tilde{w}(\varsigma) = w(\varsigma)$. After carrying out a direct star-triangle transformation [21], we get a couple of algebraic equations with two unknown parameters K_0 and K to be determined, so the algebraic system equations read as follows:

$$\tilde{w}_1 = e^{\beta K_0}\exp\left(-\frac{\beta K}{4}\right) = w_1, \tag{13}$$

$$\tilde{w}_3 = e^{\beta K_0}\exp\left(\frac{3\beta K}{4}\right) = w_3. \tag{14}$$

Subsequently, the unknown parameters of the effective triangular Ising model could be expressed in terms of arbitrary parameters of the spin-1/2 Ising-*XXZ* model on a decorated honeycomb lattice [see Eq. (1)]

$$K = \frac{1}{\beta}\ln\left(\frac{w_3}{w_1}\right), \tag{15}$$

$$K_0 = \frac{1}{4\beta}\ln\left(w_1^3 w_3\right), \tag{16}$$

where w_1 and w_3 are given by Eqs. (9) and (10), respectively.

B. Zero temperature phase diagram

Before exploring the finite temperature features, let us first study the zero-temperature phase transition when *xy* component exchange interaction J_x is taken into account. In Fig. 3 is illustrated the zero temperature phase diagram in the plane J-J_z. In Fig. 3(a), we report a typical phase diagram of the spin-1/2 Ising model on a decorated honeycomb lattice ($J_x = 0$) [18]. That is, we report one ferromagnetic (FM) phase for $J > 0$ and $J_z > 0$, another classical ferrimagnetic (CFI) phase for $J < 0$ and $J_z > 0$, and two types of ferrimagnetic ($\text{FI}^\pm$) phases for $J_z < 0$ with $J < 0$ and $J > 0$, respectively.

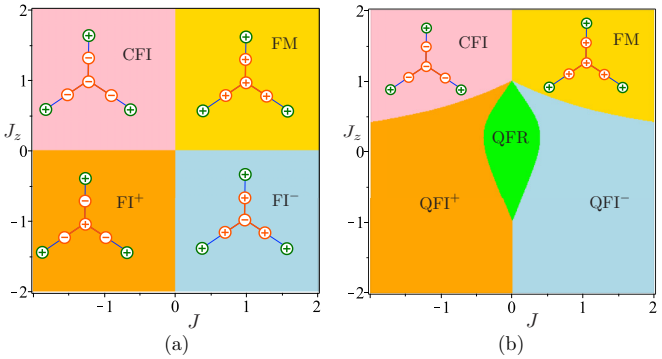

FIG. 3. Zero temperature phase diagram in the plane J-J_z. (a) For Ising model on a decorated honeycomb lattice ($J_x = 0$). (b) For Ising-XXZ model on a decorated honeycomb lattice, assuming $J_x = 1$.

Already in Fig. 3(b) is depicted the phase diagram for an Ising-XXZ model on a decorated honeycomb lattice, described by the Hamiltonian (1). The ground-state energy comes from the eigenvalues $\{\varepsilon_1^{(3)}, \varepsilon_2^{(3)}, \varepsilon_{14}^{(3)}, \varepsilon_{16}^{(3)}, \varepsilon_8^{(1)}\}$ of Table I. First, we express the ground-state energy per unit cell for ferromagnetic (FM) phase

$$E_{\mathrm{FM}} = -\frac{3}{4}(J_z + J), \tag{17}$$

and the corresponding ground state per unit cell is

$$|\mathrm{FM}\rangle \mapsto |{}_+^+\bigcirc_+^+\rangle \otimes |{}_+^+{+}_+^+\rangle. \tag{18}$$

In the direct product, the left ket corresponds to Ising spin configurations, while the second ket corresponds to the Heisenberg spin configurations. Indeed, the FM state is invariant under full spin inversion, so this state is twofold degenerate.

Let us define the magnetization for each configuration as follow: $m^I = 0.5$ for Ising spin, $m_0^H = 0.5$ for the inner Heisenberg spin, and $m_1^H = (0.5 + 0.5 + 0.5)/3 = 0.5$ for the Heisenberg spin that connects to Ising spin. Likewise, the total magnetization per unit cell may be obtained as follows:

$$m_t = \frac{m^I + m_0^H + 3m_1^H}{5}. \tag{19}$$

Thus, for the ferromagnetic case, the total magnetization obviously becomes $m_t = 0.5$.

Second, the phase diagram in Fig. 3(b) also shows a classical ferrimagnetic (CFI) phase per unit cell for $J > 0$ and $J_z < 0$, providing the result in

$$E_{\mathrm{CFI}} = -\frac{3}{4}(J_z - J). \tag{20}$$

Here, we call this a "classical" phase because the ground state is independent of the parameter J_x. Thus, the ground state per unit cell of the aforementioned energy becomes

$$|\mathrm{CFI}\rangle \mapsto |{}_-^-\bigcirc_-^-\rangle \otimes |{}_+^+{+}_+^+\rangle. \tag{21}$$

The left ket corresponds to the Ising spin setups in the direct product, whereas the second ket corresponds to the Heisenberg spin setups. Obviously, the model is invariant under global spin inversion, so the CFI state is twofold degenerate.

Note that the magnetizations are $m^I = -0.5$, $m_0^H = 0.5$, $m_1^H = 0.5$, and $m_t = 0.3$.

Furthermore, the third phase corresponds to a quantum ferrimagnetic (QFI$^-$) phase whose ground-state energy per unit cell reads

$$E_{\mathrm{QFI}^-} = \frac{1}{4}\left(J_z - 2J - \sqrt{(J - 2J_z)^2 + 12J_x^2}\right). \tag{22}$$

And corresponding ground states per unit cell is given by

$$|\mathrm{QFI}^-\rangle \mapsto \frac{|{}_+^+\bigcirc_+^+\rangle \otimes [J_x|({}_+^+{+}_-^+)\rangle + \varepsilon_{14}^{(3)}|{}_+^+{-}_+^+\rangle]}{\sqrt{3J_x^2 + (\varepsilon_{14}^{(3)})^2}}, \tag{23}$$

in direct product, the left ket corresponds to the Ising spins, whereas right ket denotes the Heisenberg spins, with $|({}_+^+s_-^+)\rangle \equiv \{|{}_+^+s_-^-\rangle + |{}_+^-s_+^+\rangle + |{}_-^+s_+^+\rangle\}$. Here, we call this "quantum" phase because the ground state and the corresponding phase depend on J_x. Since the system is invariant under global spin inversion, the QFI$^-$ state is also twofold degenerate.

In this case the magnetization can be recovered using the Eq. (71), and taking the limit of $T = 0$, which results in

$$m^I = \frac{1}{2}, \tag{24}$$

$$m_0^H = -\frac{J - 2J_z}{2\sqrt{(J - 2J_z)^2 + 12J_x^2}}, \tag{25}$$

$$m_1^H = \frac{J - 2J_z}{6\sqrt{(J - 2J_z)^2 + 12J_x^2}} + \frac{1}{3}, \tag{26}$$

$$m_t = \frac{3}{10}. \tag{27}$$

However, the magnetization of all Heisenberg spins is constant ($m_0^H + 3m_1^H = 1$), independent of Hamiltonian parameters.

The other quantum ferrimagnetic (QFI$^+$) phase arises for $J < 0$ and $J_z < 0$, whose ground-state energy per unit cell results in

$$E_{\mathrm{QFI}^+} = \frac{1}{4}\left[J_z + 2J - \sqrt{(J + 2J_z)^2 + 12J_x^2}\right]. \tag{28}$$

Whereas the ground state QFI$^+$ per unit cell becomes

$$|\mathrm{QFI}^+\rangle \mapsto \frac{|{}_-^-\bigcirc_-^-\rangle \otimes [J_x|({}_+^+{+}_-^+)\rangle + \varepsilon_{16}^{(3)}|{}_+^+{-}_+^+\rangle]}{\sqrt{3J_x^2 + \left(\varepsilon_{16}^{(3)}\right)^2}}, \tag{29}$$

in the direct product, the left ket denotes Ising spins, and the right spins correspond to the Heisenberg spins. Similar to previous states, the QFI$^+$ is invariant upon reversing all spins, so the QFI$^+$ state is again twofold degenerate.

Again using Eq. (71) and taking the limit $T = 0$, one can obtain straightforwardly the following magnetizations:

$$m^I = -\frac{1}{2}, \tag{30}$$

$$m_0^H = \frac{J + 2J_z}{2\sqrt{(J + 2J_z)^2 + 12J_x^2}}, \tag{31}$$

$$m_1^H = -\frac{J + 2J_z}{6\sqrt{(J + 2J_z)^2 + 12J_x^2}} + \frac{1}{3}, \tag{32}$$

$$m_t = \frac{1}{10}. \tag{33}$$

Analogous to the QFI$^-$ phase, the magnetization of all Heisenberg spins becomes $m_0^H + 3m_1^H = 1$, independent of the Hamiltonian parameters.

The last phase arises due to including the xy component exchange interaction J_x. This state is a quantum spin frustrated (QFR) phase, whose ground-state energy per unit cell becomes from Table I by

$$E_{\rm QFR} = \frac{1}{4}(J_z - \sqrt{B_+}), \tag{34}$$

with B_+ being defined in Eq. (5). After a bit of cumbersome algebraic manipulation, the corresponding eigenstate per unit cell results in

$$|{\rm QFR}\rangle = |_+\overset{?}{\bigcirc}_-\rangle \otimes |hAF_?\rangle, \tag{35}$$

where $? = \pm$, and

$$\begin{aligned}|hAF_+\rangle \mapsto \frac{1}{\mathcal{N}_+}[&a_2|_-\overset{-}{+}_+\rangle + a_1|_+\overset{-}{+}_-\rangle + a_1|_-\overset{+}{+}_-\rangle \\ &+b_1|_+\overset{-}{-}_+\rangle + b_1|_-\overset{+}{-}_+\rangle + b_2|_+\overset{+}{-}_-\rangle],\end{aligned} \tag{36}$$

$$\begin{aligned}|hAF_-\rangle \mapsto \frac{1}{\mathcal{N}_-}[&\bar{a}_1|_-\overset{-}{+}_+\rangle + \bar{a}_2|_+\overset{-}{+}_-\rangle + \bar{a}_1|_-\overset{+}{+}_-\rangle \\ &+\bar{b}_1|_+\overset{-}{-}_+\rangle + \bar{b}_2|_-\overset{+}{-}_+\rangle + \bar{b}_1|_+\overset{+}{-}_-\rangle],\end{aligned} \tag{37}$$

with $\mathcal{N}_+ = \sqrt{2a_1^2 + a_2^2 + 2b_1^2 + b_2^2}$, $\mathcal{N}_- = \sqrt{2\bar{a}_1^2 + \bar{a}_2^2 + 2\bar{b}_1^2 + \bar{b}_2^2}$ being the normalization coefficient. Whereas the Heisenberg spins state $|hAF_+\rangle$ coefficients are given by

$$\begin{aligned}a_1 &= J_x(\sqrt{B_+} - 3J)\big(10J^2 + J_x^2 - C^2\big) + \frac{2J}{J_x}b_1, \\ a_2 &= J_x(\sqrt{B_+} - 3J)\big(C^2 + 2J^2 - 5J_x^2\big), \\ b_2 &= 4\big(3J^2 - J_x^2\big)\big(C^2 + 2J^2 - J_x^2\big) + \frac{2J}{J_x}a_2, \\ b_1 &= 8J_x^2\big(3J^2 - J_x^2\big),\end{aligned} \tag{38}$$

where $C^2 = \sqrt{(2J^2 + 3J_x^2)^2 + 16J^2J_x^2}$, and for $|hAF_-\rangle$ becomes

$$\begin{aligned}\bar{a}_1 &= J_x(\sqrt{B_+} + 3J)\big(10J^2 + J_x^2 - C^2\big) - \frac{2J}{J_x}\bar{b}_1, \\ \bar{a}_2 &= J_x(\sqrt{B_+} + 3J)\big(C^2 + 2J^2 - 5J_x^2\big), \\ \bar{b}_2 &= 4\big(3J^2 - J_x^2\big)\big(C^2 + 2J^2 - J_x^2\big) - \frac{2J}{J_x}\bar{a}_2, \\ \bar{b}_1 &= 8J_x^2\big(3J^2 - J_x^2\big).\end{aligned} \tag{39}$$

It should be noted that if $J \mapsto -J$, the following property must held $a_1 \leftrightarrows b_1$ and $a_2 \leftrightarrows b_2$, and equivalently for $\bar{a}_1 \leftrightarrows \bar{b}_1$ and $\bar{a}_2 \leftrightarrows \bar{b}_2$.

Note that the magnetization $m^I = 0$, $m_0^H = 0$, and $m_1^H = 0$, then $m_t = 0$. This result could be confirmed from Eqs. (70) and (71).

In Fig. 4 is illustrated a frustrated Ising spin arrangement for the spin-1/2 Ising model on the triangular lattice. In this arrangement, two vertices of the triangle have two opposite spins, and the third spin must take at random upward or downward. We can also check that six spins surround each random spin by alternating fixed spins.

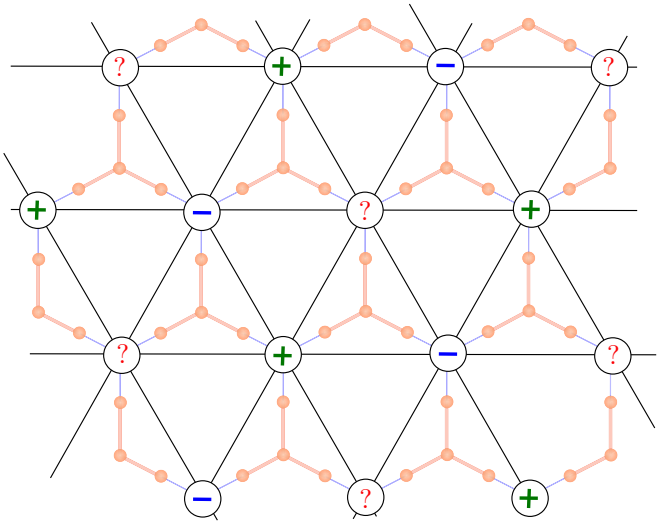

FIG. 4. A schematic arrangement of spin frustration in the effective triangular lattice.

Indeed, the probability amplitude of the Heisenberg spins state is somewhat cumbersome to be inspected quickly, so let us analyze some limiting cases:

(i) First, we consider a trivial case when $J = 0$, so the QFR state reduces to

$$\begin{aligned}|{\rm QFR}\rangle \mapsto \frac{1}{\sqrt{6}}|_+\overset{?}{\bigcirc}_-\rangle \otimes [&|_-\overset{-}{+}_+\rangle + |_+\overset{-}{+}_-\rangle + |_-\overset{+}{+}_-\rangle \\ &+ |_+\overset{-}{-}_+\rangle + |_-\overset{+}{-}_+\rangle + |_+\overset{+}{-}_-\rangle],\end{aligned} \tag{40}$$

where each spin configuration are equally probably, since there is no exchange interaction with Ising spins.

(ii) The second case we consider is when $J > 0$ and $J_x \to 0$, then for this purpose, we take the Taylor expansion in Eq. (38) around $J_x = 0$ up to order $\mathcal{O}(J_x^4)$. Therefore, the coefficients simply become

$$\begin{aligned}a_1 &= \frac{J_x}{J} - \frac{5}{2}\Big(\frac{J_x}{J}\Big)^3, \quad \bar{a}_1 = -\frac{J_x}{J} - \frac{5}{2}\Big(\frac{J_x}{J}\Big)^3, \\ a_2 &= \frac{1}{3}\Big(\frac{J_x}{J}\Big)^3, \quad \bar{a}_2 = -\frac{1}{3}\Big(\frac{J_x}{J}\Big)^3, \\ b_2 &= 1 - \Big(\frac{J_x}{J}\Big)^2, \quad \bar{b}_2 = 1 - \Big(\frac{J_x}{J}\Big)^2, \\ b_1 &= \Big(\frac{J_x}{J}\Big)^2, \quad \bar{b}_1 = \Big(\frac{J_x}{J}\Big)^2.\end{aligned} \tag{41}$$

It is obvious that the coefficients hold the aforementioned property when $J \mapsto -J$.

Note that for exactly $J_x = 0$ (Ising model on a decorated honeycomb lattice [18]), the only coefficient that survives is b_2, thus the frustrated state reduces to $|{\rm QFR}\rangle \mapsto |_+\overset{+}{\bigcirc}_-\rangle \otimes |_-\overset{+}{-}_+\rangle$ or $|_+\overset{-}{\bigcirc}_-\rangle \otimes |_+\overset{-}{-}_+\rangle$, but the eigenvalue (34) is no longer the ground-state energy, unless in a trivial case when $J_z = 0$. So that the quantum spin frustrated state vanishes, thereby

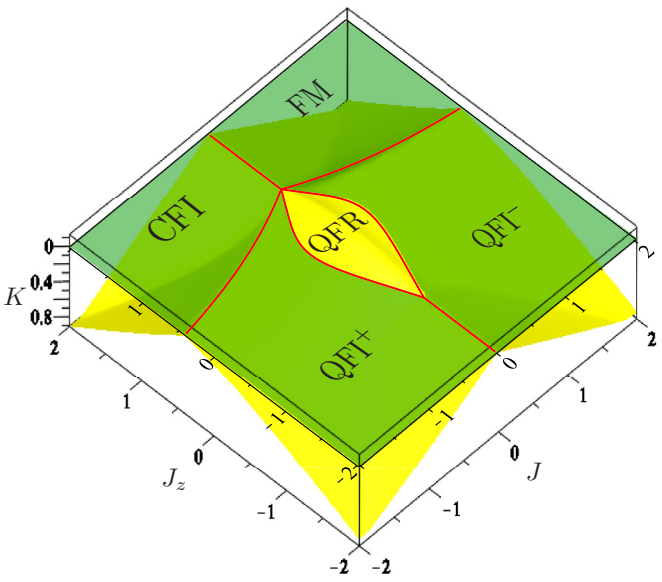

FIG. 5. The effective interaction K given by Eq. (15) by a yellow surface as a function of J and J_z, assuming fixed $J_x = 1$. Transparent green plane corresponds to $K = 0$, the negative K is illustrated on the top of surface for convenience.

confirming the absence of quantum spin frustration of the spin-1/2 Ising model on a decorated honeycomb lattice [18].

Another thing we point out is the absence of symmetry under local Heisenberg spin reversal. Since $a_1 \neq b_1$ and $a_2 \neq b_2$, this is already manifest in the coefficients provided in Eq. (38), which is even more evident in the amplitude probability of Eqs. (41).

It is worth remarking that the QFR phase exclusively arises due to the J_x contribution. This means that in the effective triangular lattice, the J_x is responsible for generating the non-fitting antiferromagnetic arrangement on triangular lattice of the Ising spins [40]. Once 1/3 of Ising spins are set to point down, other 1/3 Ising spins are set to point up, while the remaining 1/3 must point up or down randomly as depicted in Fig. 4. This configuration gains a weight of $2^{1/3}$ per spin, and in addition, there is still a considerable amount of contingent freedom to be taken into account. Because random spins can vary independently; thus three random spins forming a triangle could often occur with the same signs (for detail, see Ref. [40]).

It is also important to note that the phase boundary curves described in Figs. 3(b) and 5 are reported by

$$\mathrm{QFI}^{+} - \mathrm{QFR}, \ \rightarrow \ J_z = \frac{-J \pm \sqrt{(2J + \sqrt{B_+})^2 - 12J_x^2}}{2}, \quad (42)$$

$$\mathrm{QFI}^{-} - \mathrm{QFR}, \ \rightarrow \ J_z = \frac{J \pm \sqrt{(2J - \sqrt{B_+})^2 - 12J_x^2}}{2}, \quad (43)$$

$$\mathrm{QFI}^{-} - \mathrm{FM}, \ \rightarrow \ J_z = \frac{\sqrt{J^2 + 4J_x^2} - J}{4}, \quad (44)$$

$$\mathrm{QFI}^{+} - \mathrm{FM}, \ \rightarrow \ J_z = \frac{\sqrt{J^2 + 4J_x^2} + J}{4}. \quad (45)$$

In Fig. 5 the effective parameter K is illustrated as a yellow surface in the plane J-J_z for a fixed $J_x = 1$ and at zero temperature. Just for convenience, in order to show a slight negative K on the top of the surface, the parameter K increases while going down, so confirming the existence of a frustrated region. At the same time, the transparent green flat region corresponds to $K = 0$.

We leave the analysis of residual entropy of the frustrated region, to next section, because to obtain this result, we need to use the free energy at finite temperature.

III. THERMODYNAMICS

Now we are in a position to discuss the thermodynamics of the present model. So the first thing to do is to get the free energy per unit cell of the model, which could be written as

$$f_{\mathrm{dh}} = -K_0 + \tilde{f}_{\mathrm{t}}, \quad (46)$$

where f_{t} denotes the free energy of the Ising model in the effective triangular lattice [18,41,42], and K_0 can be understood as an effective "constant" energy of the effective triangular lattice, since it is independent of spins on a triangular lattice but depends of the temperature.

Consequently, the free energy of effective triangular lattice per unit cell [18,41,42] could be expressed using a single integral [43,44], as follows:

$$f_{\mathrm{t}} = \frac{T}{4}\ln(r) - \frac{T}{4\pi}\int_{-\pi}^{\pi} \ln[\mathcal{A}(\phi) + \sqrt{\mathcal{Q}(\phi)}]d\phi, \quad (47)$$

where $\mathcal{A}(\phi)$ and $\mathcal{Q}(\phi)$ are defined by

$$\mathcal{A}(\phi) = \tfrac{1}{2}r^2 + \tfrac{3}{2} + (1-r)\cos(\phi), \quad (48)$$

$$\mathcal{Q}(\phi) = \mathcal{A}(\phi)^2 - 2(r-1)^2[1 + \cos(\phi)], \quad (49)$$

with $r = \frac{w_3}{w_1}$. Thus, the free energy per unit cell of decorated triangular lattice becomes

$$f_{\mathrm{dh}} = -T\ln(w_1) - \frac{T}{4\pi}\int_{-\pi}^{\pi} \ln[\mathcal{A}(\phi) + \sqrt{\mathcal{Q}(\phi)}]d\phi. \quad (50)$$

Alternatively, let us define the following quantity:

$$u = \frac{2(1-r)}{r^2+3}, \quad \text{where} \quad -\frac{1}{3} < u \leqslant \frac{2}{3}. \quad (51)$$

Using this relation, the free energy can be re-expressed as follows:

$$f_{\mathrm{dh}} = -\frac{T}{2}\ln\left(\frac{w_3^2 + 3w_1^2}{2}\right) - \frac{T}{4}\left\{\ln\left[\frac{2-u^2}{4} + \frac{\sqrt{1-u^2}}{2}\right]\right\} - \frac{T}{4\pi}\int_{-\pi}^{\pi} \ln[1 + \sqrt{1-\kappa(\phi)^2}]d\phi, \quad (52)$$

where

$$\kappa(\phi) = \frac{u\sqrt{2[1+\cos(\phi)]}}{[1 + u\cos(\phi)]}. \quad (53)$$

Before further investigation concerning thermodynamic properties, two interesting cases should be noted.

First, we analyze the residual entropy in the QFR region, which occurs when $w_3 < w_1$ and assuming $T \to 0$, this implies that $r = \frac{w_3}{w_1} \to 0$, then the Eqs. (48) and (49) reduce to

$$\mathcal{A}(\phi) = \cos(\phi) + \tfrac{3}{2}, \quad (54)$$

$$\mathcal{Q}(\phi) = \left[\cos(\phi) + \tfrac{3}{2}\right]^2 - 2[1 + \cos(\phi)], \quad (55)$$

both functions are independent of T and r, then after some algebraic manipulation, the residual entropy results in

$$\begin{aligned}\mathcal{S} &= \frac{1}{3}\ln(2) + \frac{1}{4\pi}\int_{-\frac{2\pi}{3}}^{\frac{2\pi}{3}} \ln\left[\cos(\phi)+1\right]d\phi,\\ &= \frac{2}{\pi}\int_{0}^{\frac{\pi}{3}} \ln\left[2\cos(\phi)\right]d\phi,\\ &= 0.32306594721945. \end{aligned} \tag{56}$$

As mentioned above, the residual entropy arises because of the contribution of the quantum exchange interaction J_x, turning the effective K of triangular lattice becoming antiferromagnetic ($K < 0$) since $r \to 0$, which implies that the model exhibits a frustrated state. This result is precisely the same residual entropy found by Wannier [40] for the nonfitting antiferromagnetic lattice.

Second, we study the residual entropy when $\frac{w_3}{w_1} = r = 1$ and $T \to 0$. In this case, we have $A(\phi) = 2$ and $\mathcal{Q}(\phi) = 2^2$, so the free energy merely reduces to

$$f_{\rm dh} = -T\ln(w_1) - \frac{T}{4\pi}\int_{-\pi}^{\pi} \ln(2^2)d\phi, \tag{57}$$

implying that residual entropy becomes $\mathcal{S} = \ln(2)$. This residual entropy emerges in the straight line given by $J = 0$ and in the phase boundary between QFR $-$ QFI$^{\pm}$, illustrated in Fig. 5 by red curves.

It is easy to convince that for QFI$^{\pm}$, CFI, and FM states we have $w_3 > w_1$ and assuming $T \to 0$, which implies that $r = \frac{w_3}{w_1} \to \infty$, thus as expected the corresponding residual entropy becomes null.

Now, once we have free energy, we return to explore the thermodynamic properties, it is possible to study several physical quantities of the Ising-*XXZ* model on a decorated honeycomb lattice. Thus, in Fig. 6 (top) is depicted the entropy as a function of J_z, assuming fixed $J_x = 1$ and $J = 1$ for a number of fixed temperatures given inside the panel. Particularly, let us start paying attention to the temperature $T = 0.005$; essentially, we observe three peaks at $J_z = -0.38$, $J_z = 0.63$, and $J_z = 0.88$ due to the influence of phase transitions at zero temperature in QFI$^-$ $-$ QFR, QFR $-$ QFI$^-$, and QFI$^-$ $-$ FM, respectively. Those peaks broaden as soon as the temperature increases. In contrast, the dashed line corresponds to the entropy $\mathcal{S}_c$ at the critical point as a function of J_z. In Fig. 6 (bottom), we illustrate the specific heat as a function of J_z, for the same set of entropy parameters. Once again, let us focus at the low-temperature region say $T = 0.005$, the sharp "peaks" actually describes the logarithmic divergence due to the second order phase transition. Meanwhile, the small double peaks that appear around the phases QFI$^-$ $-$ QFR ($J_z = -0.38$), QFR $-$ QFI$^-$ ($J_z = 0.63$), and QFI$^-$ $-$ FM ($J_z = 0.88$), correspond to the phase transition effect at zero temperature. Of course, these anomalous peaks vanish as the temperature increases, surviving only the logarithmic divergence at the critical temperature T_c.

In Fig. 7 (top) is reported the entropy as a function of J_x, for fixed $J_z = 1$, $J = 0.025$, and assuming several values of temperature $T = \{0.005, 0.015, 0.02, 0.025, 0.034, 0.05\}$. For temperature $T = 0.005$, again, we observe two peaks, and the sharper peak arises as a consequence of zero temperature phase transition between QFI$^-$ $-$ FM ($J_x = 1.118$), while the broader peak indicates the influence of zero temperature phase transition between QFI$^-$ $-$ QFR ($J_x = 1.369$). When the temperature increases, the influence of the zero-temperature phase transition, shows that the peaks vanish. Meanwhile, the dashed line describes entropy $\mathcal{S}_c$ at critical temperature as a function of J_x. In Fig. 7 (bottom) is shown the specific heat as a function of J_x for the same set of param-

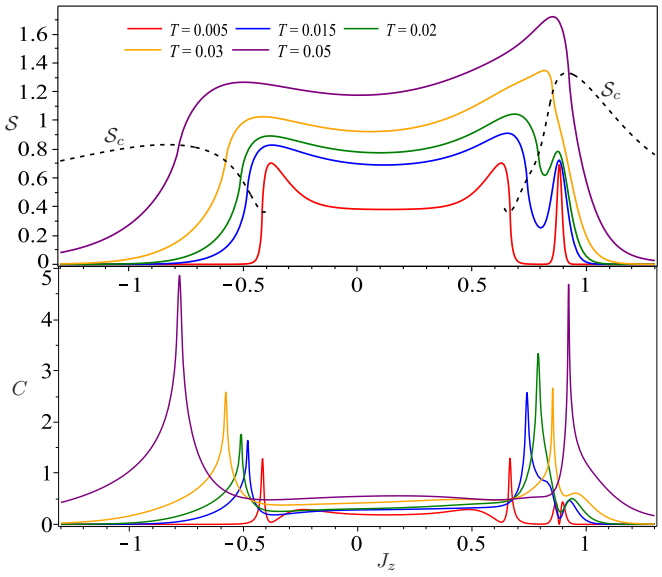

FIG. 6. (Top) Entropy $\mathcal{S}$ as a function of J_z, assuming $J_x = 1$, $J = 0.025$ and for fixed temperatures $T = \{0.005, 0.015, 0.02, 0.03, 0.05\}$, dashed line corresponds to the entropy at critical point. (Bottom) Specific heat as a function of J_z for the same set of parameters of the top panel.

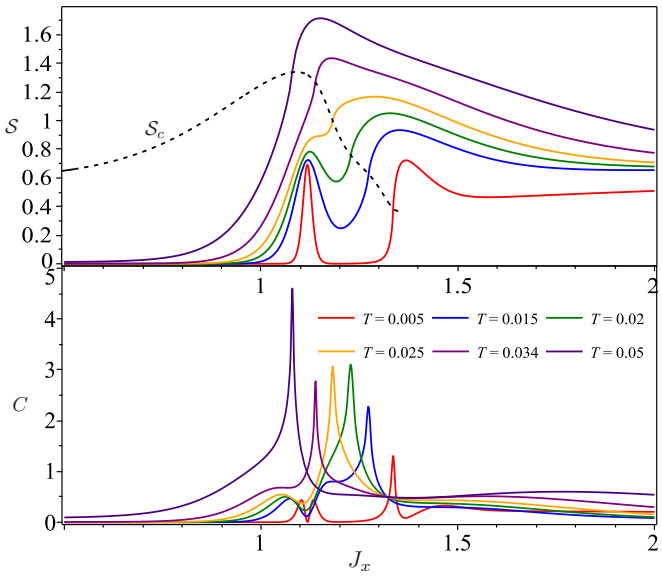

FIG. 7. (Top) Entropy $\mathcal{S}$ as a function of J_x, assuming $J_z = 1$, $J = 0.025$ and for fixed temperatures $T = \{0.005, 0.015, 0.02, 0.025, 0.034, 0.05\}$. (Bottom) Specific heat as a function of J_x, for the same set of parameters of entropy.

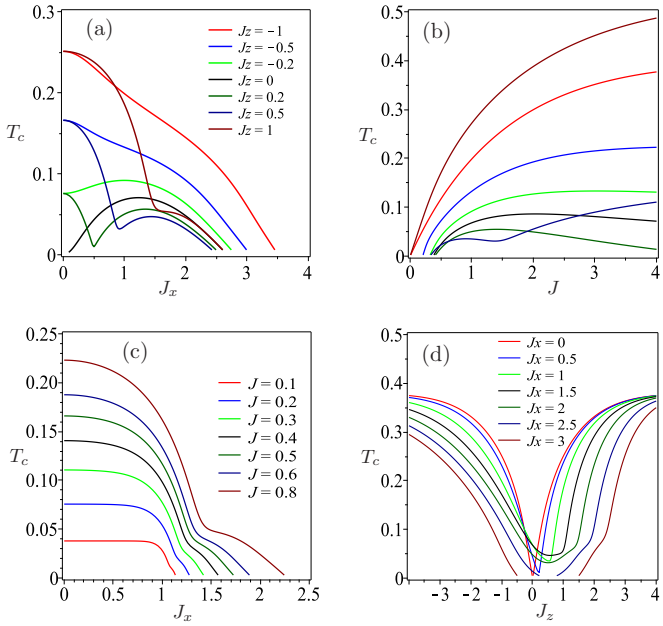

FIG. 8. (a) Critical temperature T_c as a function of J_x, for fixed $J = 1$ and certain values of J_z. (b) Critical temperature T_c as a function of J, for a range of values in J_z and fixed $J_x = 1$. (c) Critical temperature T_c as a function of J_x, for several values of J assuming fixed $J_z = 1$. (d) Critical temperature T_c as a function of J_z, for certain values of J_x and fixed $J = 1$.

eters considered for entropy. Although once more, for $T = 0.005$ we observe a double peak around the zero-temperature phase transition QFI$^-$ − FM. This double peak disappears in the same way as in the previous case when the temperature increases. We also observe at the critical temperature a logarithmic divergence for each curve, corresponding to the second-order phase transition.

A. Critical temperature

In the following, we will discuss one of the most significant properties of 2D lattice models, the critical behavior at finite temperature. It is well established that the critical temperature of the spin-1/2 Ising model on the triangular lattice is given by $\frac{K}{T_c} = \ln(3)$ [18,45]. Consequently, we can write the critical condition as follows:

$$\frac{w_3^c}{w_1^c} = r_c = 3, \tag{58}$$

where w_1^c and w_3^c refer to the Boltzmann factors at a critical temperature T_c, given by Eqs. (9) and (10) at $T = T_c$, respectively. An explicit expression involves a huge algebraic expression, which is irrelevant to write explicitly here.

In Fig. 8(a) is illustrated the critical temperature T_c as a function of J_x for several values of J_z and fixing $J = 1$. For $J_z > 0$ we observe an interesting behavior where appears a minimum, which corresponds to the interface between QFR and QFI$^{\pm}$, although for $J_z = 0$ there is a special curve with two critical points at zero temperature (for detail see Fig. 3). For $|J_z| \gtrsim 0.2$ only occurs one critical point at zero temperature. Furthermore, Fig. 8(b) depicts the critical temperature as a function of J, assuming $J_x = 1$ and the same set of

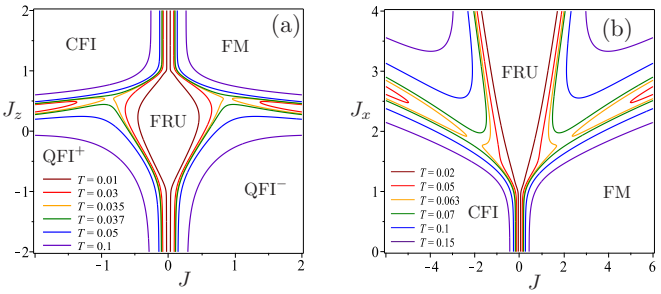

FIG. 9. (a) Isothermal curves in the plane J-J_z, for fixed $J_x = 1$ and a number of fixed temperature T as denoted inside. (b) Isothermal curves in the plane J-J_x, for fixed $J_z = 1$ and several fixed temperature T reported inside the panel.

parameters for J_z considered in Fig. 8(a). Similarly, in Fig. 8(c), the critical temperature is depicted as a function of J_z, keeping fixed $J_z = 1$, and for a range of values of J as displayed inside the panel. Finally, Fig. 8(d) illustrates the critical temperature as a function of J_z assuming fixed $J = 1$ and for a set of values of J_x. For the parameter $J_x \lesssim 2.5$, the critical temperature has a minimum indicating the vestiges of transition between QFI$^-$ and QFI$^+$, the minimum disappears for $J_x > 2.5$.

In Fig. 9(a) is reported the isothermal curves in the plane J-J_z, keeping fixed $J_x = 1$. Here, we can identify the influence of the zero-temperature phase diagram for several temperature values. For detail, compare with Fig. 3(b). Likewise, Fig. 9(b) displays the isothermal curves in the plane J-J_x, considering fixed $J_z = 1$, and for a set of temperatures reported inside the panel.

B. Spontaneous magnetization

Another important quantity to be analyzed herein is the magnetic property of the present model. That is why we need to examine the magnetization of the decorated Ising-*XXZ* lattice. The Ising spin magnetization $m^I = \langle s \rangle$ could be determined according to the magnetization of the effective Ising model on a 2D triangular lattice. In contrast, the magnetization of Heisenberg spins can be provided using the generalized star-triangle transformation approach [17–19,21]

$$\langle \sigma_k^z \rangle = \eta_k \langle s_1 \rangle + \frac{\gamma_k}{3} \langle s_1 s_2 s_3 \rangle, \quad \text{with} \quad k = \{0, 1\}, \tag{59}$$

which combines the single Ising spins thermal average $\langle s \rangle$ and triple Ising spins $\langle s_1 s_2 s_3 \rangle$ linearly. Hence, we denote by $m_0^H = \langle \sigma_0^z \rangle$ the central Heisenberg spin magnetization, and $m_1^H = \langle \sigma_1^z \rangle$ means the outer (decorated) Heisenberg spin magnetization. To find the coefficients η_k and γ_k, we use the following relation [17–19,21]:

$$\zeta\left(\varsigma, \sigma_k^z\right) = [\eta_k (s_1 + s_2 + s_3) + \gamma_k s_1 s_2 s_3] w(\{\boldsymbol{\sigma}, s\}). \tag{60}$$

Analogously, for the Ising-*XXZ* model on a decorated honeycomb lattice might be expressed as

$$\tilde{\zeta}\left(\sigma_k^z\right) = \mathrm{tr}_{\{\sigma\}}\left[\hat{\sigma}_k^z \mathbf{V}(\{\boldsymbol{\sigma}, s\})\right]. \tag{61}$$

However, the Ising spin coupling configurations $\{+++\}$ and $\{++-\}$, are denoted merely as $\tilde{\zeta}(1/2, \sigma_k^z) = \tilde{\zeta}_1(\sigma_k^z)$ and $\zeta(3/2, \sigma_k^z) = \zeta_3(\sigma_k^z)$. Therefore, these coefficients should be

expressed as follows:

$$\tilde{\zeta}_3(\sigma_k^z) = \mathrm{tr}_{\{\sigma\}}\left[\mathbf{U}_3 \hat{\sigma}_k^z \mathbf{U}_3^{-1} \boldsymbol{\lambda}_3\right], \tag{62}$$

$$\tilde{\zeta}_1(\sigma_k^z) = \mathrm{tr}_{\{\sigma\}}\left[\mathbf{U}_1 \hat{\sigma}_k^z \mathbf{U}_1^{-1} \boldsymbol{\lambda}_1\right], \tag{63}$$

where the orthogonal matrices $\mathbf{U}_3$ and $\mathbf{U}_1$ are obtained directly from the corresponding eigenvectors of the eigenvalues provided in Table I, for each configuration $\{+++\}$ and $\{++-\}$, respectively. Although, here, we do not explicitly write the matrices $\mathbf{U}_3$ and $\mathbf{U}_1$, because their dimensions are 16×16, and most elements of the matrices are huge expressions. Thus, it is unnecessary to write down here explicitly the matrices $\mathbf{U}_3$ and $\mathbf{U}_1$, but we can easily generate them in algebraic programs.

From Eq. (60) we also have the following relations:

$$\zeta_3(\sigma_k^z) = \left(\tfrac{3}{2}\eta_k + \tfrac{1}{8}\gamma_k\right) w_3, \tag{64}$$

$$\zeta_1(\sigma_k^z) = \left(\tfrac{1}{2}\eta_k - \tfrac{1}{8}\gamma_k\right) w_1. \tag{65}$$

Hence, the unknown coefficients result in

$$\eta_k = \frac{1}{2}\left[\frac{\zeta_3(\sigma_k^z)}{w_3} + \frac{\zeta_1(\sigma_k^z)}{w_1}\right], \tag{66}$$

$$\gamma_k = 2\left[\frac{\zeta_3(\sigma_k^z)}{w_3} - 3\frac{\zeta_1(\sigma_k^z)}{w_1}\right], \tag{67}$$

with $\zeta_3(\sigma_k^z) = \tilde{\zeta}_3(\sigma_k^z)$ and $\zeta_1(\sigma_k^z) = \tilde{\zeta}_1(\sigma_k^z)$. Here $\tilde{\zeta}_3(\sigma_k^z)$ and $\tilde{\zeta}_1(\sigma_k^z)$ are given by Eqs. (62) and (63), respectively.

Furthermore, the thermal average relationship of single and triple Ising spins was found in Ref. [45] which is rewritten as follows:

$$\langle s_1 s_2 s_3 \rangle = G(r)\langle s_1 \rangle, \tag{68}$$

where $G(r)$ after some algebraic manipulation becomes

$$G(r) = \frac{3r^2 - 3 - 2r\sqrt{(r-1)(r+3)}}{4(r-1)^2}. \tag{69}$$

Moreover, the thermal average of Ising spin $\langle s_1 \rangle$ [45] is given by

$$\langle s_1 \rangle = \begin{cases} \frac{1}{2}\left[\frac{(r-3)(r+1)^3}{(r+3)(r-1)^3}\right]^{\frac{1}{8}}, & r > 3, \\ 0, & 0 < r \leqslant 3. \end{cases} \tag{70}$$

Therefore, the thermal average of Heisenberg spins for both expressions can be derived by using the following relation:

$$\langle \sigma_k^z \rangle = \left\{\left(\frac{3}{2} + 2G\right)\frac{\zeta_3(\sigma_k^z)}{w_3} + \left(\frac{3}{2} - 6G\right)\frac{\zeta_1(\sigma_k^z)}{w_1}\right\}\langle s_1 \rangle. \tag{71}$$

Note that the magnetization exponent satisfies the same universality class of the two-dimensional Ising model, because all Ising ferromagnets in two-dimensional have the same critical exponent of $1/8$, regardless of lattice.

The zero-temperature Heisenberg spin magnetization for the QFI$^{\pm}$ regions occurs when $r \to \infty$, which means $G(\infty) = 1/4$. Under this condition simplifying Eq. (71), we have

$$m_k^H = \lim_{r\to\infty} \frac{\zeta_3(\sigma_k^z)}{w_3}\langle s_1 \rangle = \begin{cases} -\frac{J_\pm + 2J_z}{\sqrt{A_\pm}}\langle s_1 \rangle, & k = 0, \\ \left(\frac{J_\pm + 2J_z}{3\sqrt{A_\pm}} \mp \frac{2}{3}\right)\langle s_1 \rangle, & k = 1, \end{cases} \tag{72}$$

where $\pm$ corresponds to QFI$^{\pm}$, respectively, and $\langle s_1 \rangle = \frac{1}{2}$.

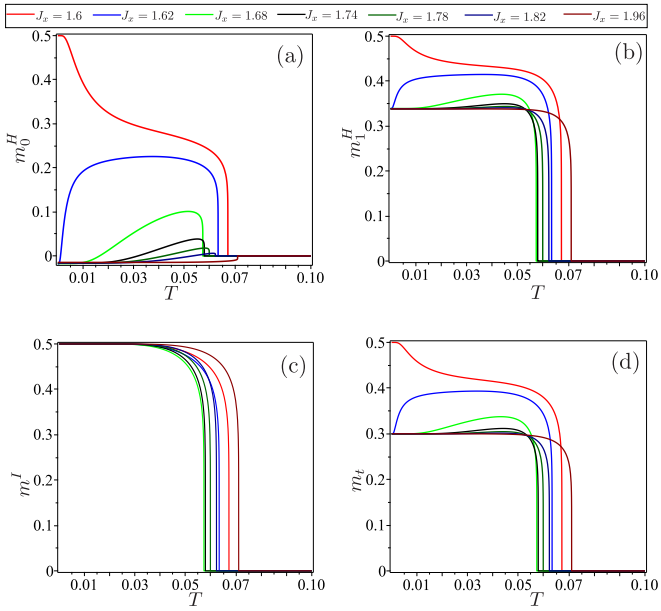

FIG. 10. (a) Heisenberg spin magnetization m_0^H as a function of temperature assuming fixed $J = 2$, $J_z = 0.9$, and for several values of J_x. (b) Heisenberg spin magnetization m_1^H as a function of temperature for the same set of parameters in panel (a). (c) Ising spin magnetization m^I as a function of temperature, assuming the same set of parameters considered in panel (a). (d) Total spin magnetization m_t as a function of temperature for the parameters considered in panel (a).

In Fig. 10(a) is depicted the central Heisenberg spin magnetization m_0^H as a function of temperature, assuming fixed $J = 2$, $J_z = 0.9$, and for several values of J_x, as described at the top of the panels. The zero-temperature magnetization for central Heisenberg spins is given by Eq. (72) for $J = 2$, $J_z = 0.9$ the curves leads to $m_0^H = -\frac{1}{2}\sqrt{\frac{3}{4J_x^2+3}}$. Whereas in Fig. 10(b) is illustrated the Heisenberg spin magnetization m_1^H which bonds with Ising spin as a function of temperature. The zero temperature magnetization is obtained from Eq. (72) for $J = 2, J_z = 0.9$ leading to $m_1^H = (\frac{1}{6}\sqrt{\frac{3}{4J_x^2+3}} + \frac{1}{3})$. In Fig. 10(c) is depicted the Ising spin magnetization $m^I = \langle s_1 \rangle$ as a function of temperature. So basically, observe a typical spontaneous magnetization of the 2D Ising model. Finally, In Fig. 10(d), we observe the total spin magnetization m_t as a function of temperature.

Another remarkable feature to note is the magnetization m_0^H for the compensation temperature T_{comp}.

Such anomalous behavior can be obtained by considering that Eq. (71) is null and setting $r > 3$. For simplicity, let us define $t_k = \frac{\zeta_3(\sigma_k^z)}{\zeta_1(\sigma_k^z)}$, and writing in terms of r and t_k we have

$$t_k = \frac{\frac{3}{2} - 6G}{\frac{3}{2} + 2G} r. \tag{73}$$

By simplifying relation (73), we get the following identity:

$$3r^2 t_k + 2r t_k^2 - 3t_k^2 - 9t_k - 9 = 0. \tag{74}$$

In particular, this requirement is only fulfilled for $k = 0$, as shown in Fig. 10(a).

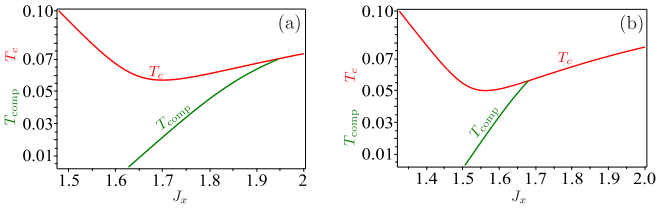

FIG. 11. Compensation temperature for central Heisenberg spin magnetization m_0^H as a function of J_x, and fixed $J = 2$. (a) For $J_z = 0.9$, and in panel (b) for $J_z = 0.8$.

The compensation temperature is also explored in Fig. 11 as a function of J_x. Figure 11(a) depicts for fixed values $J = 2$, $J_z = 0.9$, and Fig. 11(b) illustrates assuming $J = 2$, $J_z = 0.8$. The central spin magnetization m_0^H has a peculiar behavior, where we observe a compensation temperature T_{comp} when the magnetization m_0^H becomes null. In both cases of Fig. 11, the compensation temperature of m_0^H vanishes as soon as the critical temperature is reached.

IV. CONCLUSION

The two-dimensional spin-1/2 Ising-Heisenberg model in a decorated honeycomb lattice with Ising and Heisenberg type exchange interaction constitutes alternating clusters in the decorated honeycomb lattice. We have verified that we can solve this model exactly through a generalized star-triangle transformation. The relevance of this model is its close relationship to the fully spin-1/2 Heisenberg model on a honeycomb lattice, since four of five particles in each unit cell are of the Heisenberg spins. Initially, we study the zero-temperature phase diagram and found a typical ferromagnetic phase (FM), one classical ferrimagnetic phase CFI, two types of quantum ferrimagnetic phases (QFI^+ and QFI^-), and one quantum spin frustrated phase (QFR). It is worth noting that the QFR states originates exclusively due to J_x exchange interaction, which corresponds to nonfitting antiferromagnetic Ising model in effective triangular lattice.

Additionally, we explored certain relevant quantities such as the zero-temperature phase diagram, thermodynamics, spontaneous magnetization, and critical temperature under several conditions of the effective spin-1/2 Ising model on a triangular lattice.

Most of our investigation is focused on the quantum spin frustrated region. The Heisenberg exchange interaction strongly influences the critical temperature, and this occurs mainly in the low-temperature region. We also obtain the residual entropy for the quantum spin frustrated region by taking zero-temperature, which coincides with the residual entropy found by Wannier [40] for the Ising model on the triangular lattice. Similarly, we derive the zero-temperature magnetization due to the existence of the quantum exchange interaction.

ACKNOWLEDGMENTS

This work was partially supported by Brazilian agencies FAPEMIG APQ-0302617 and CNPq 312379/2021-8.

[1] L. Onsager, Phys. Rev. **65**, 117 (1944).
[2] F. Y. Wu, J. Math. Phys. **15**, 687 (1974).
[3] T. Horiguchi, Phys. Lett. A **113**, 425 (1986).
[4] M. Kolesik and L. Samaj, Int. J. Mod. Phys. B **06**, 1529 (1992).
[5] F. Y. Wu, J. Phys. A: Math. Gen. **23**, 375 (1990).
[6] P. Azaria and H. Giacomini, J. Phys. A: Math. Gen. **21**, L935 (1988).
[7] W. T. Lu and F. Y. Wu, Phys. Rev. E **71**, 046120 (2005).
[8] L. Song, L. Zhang, Y. Guan, H. Zhao, X. Xu, J. Lu, C. Yan, and J. Cai, Mater. Res. Express **6**, 075911 (2019)
[9] P. Sang, Q. Wang, W. Wei, F. Wang, Y. Li, and J. Chen, ACS Materials Lett. **3**, 1181 (2021).
[10] T. Zhang and L. Zhu, Phys. Chem. Chem. Phys. **23**, 1292 (2021).
[11] T. Mizoguchi, Y. Kuno, and Y. Hatsugai, Phys. Rev. A **102**, 033527 (2020).
[12] L. Zhang, S. Zhang, W. Ji, C. Zhang, P. Li, P. Wang, S. Li, and S. Yan, Nanoscale **10**, 20748 (2018).
[13] L. Zhang, C. Zhang, S. Zhang, W. Ji, P. Li, and P. Wang, Nanoscale **11**, 5666 (2019).
[14] Y. Ding and Y. Wang, Phys. Chem. Chem. Phys. **20**, 6830 (2018).
[15] M. P. Shores, E. A. Nytko, B. M. Bartlett, and D. G. Nocera, J. Am. Chem. Soc. **127**, 13462 (2005).
[16] T. H. Han, J. S. Helton, S. Y. Chu, D. G. Nocera, J. A. Rodriguez-Rivera, C. Broholm, and Y. S. Lee, Nature (London) **492**, 406 (2012).
[17] M. E. Fisher, Phys. Rev. **113**, 969 (1959).
[18] I. Syozi, in *Phase Transitions and Critical Phenomena*, edited by C. Domb and M. S. Green (Academic Press, New York, 1972), Vol. 1.
[19] O. Rojas, J. S. Valverde, and S. M. de Souza, Physica A **388**, 1419 (2009).
[20] J. Strečka, Phys. Lett. A **374**, 3718 (2010).
[21] O. Rojas and S. M. de Souza, J. Phys. A: Math. Theor. **44**, 245001 (2011).
[22] M. Rojas, O. Rojas, and S. M. de Souza, Phys. Rev. E **86**, 051116 (2012).
[23] O. Rojas, J. Magn. Magn. Mater. **473**, 442 (2019).
[24] Y. L. Loh, D. X. Yao, and E. W. Carlson, Phys. Rev. B **77**, 134402 (2008).
[25] J. Strečka, L. Canova, M. Jascur, and M. Hagiwara, Phys. Rev. B **78**, 024427 (2008).
[26] J. Torrico, J. Strečka, O. Rojas, S. M. de Souza, and M. L. Lyra, Phys. Rev. E **101**, 032104 (2020).
[27] J. S. Valverde, O. Rojas, and S. M. de Souza, Phys. Rev. E **79**, 041101 (2009).
[28] K. Y. Lin and J. L. Chen, J. Phys. A: Math. Gen. **20**, 5695 (1987).
[29] J. H. Barry and M. Khatun, Phys. Rev. B **51**, 5840 (1995).
[30] Y. Tang, C. Peng, W. Guo, J. Wang, G. Su, and Z. He, J. Am. Chem. Soc. **139**, 14057 (2017).
[31] L. Galisova and M. Kaczor, Entropy **23**, 1671 (2021).
[32] L. Galisova, J. Phys.: Condens. Matter **31**, 465801 (2019)

[33] J. Čisárová and J. Strecka, Phys. Rev. B **87**, 024421 (2013).
[34] J. Čisárová, F. Michaud, F. Mila, and J. Strecka, Phys. Rev. B **87**, 054419 (2013).
[35] H. A. Zad and J. Strečka, Phys. Rev. E **105**, 044115 (2022).
[36] J. Strečka and C. Ekiz, Phys. Rev. E **91**, 052143 (2015).
[37] J. Strečka and C. Ekiz, Phys. Rev. E **102**, 012132 (2020).
[38] J. Richter, J. Shukenburg, A. Honecker, and D. Schmalfuß, Phys. Rev. B **70**, 174454 (2004).
[39] B. J. Yang, A. Paramekanti, and Y. B. Kim, Phys. Rev. B **81**, 134418 (2010).
[40] G. H. Wannier, Phys. Rev. **79**, 357 (1950).
[41] K. Kano and S. Naya, Prog. Theor. Phys. **10**, 158 (1953).
[42] P. Azaria, H. T. Diep, and H. Giacomini, Phys. Rev. Lett. **59**, 1629 (1987).
[43] C. Fan and F. Wu, Phys. Rev. B **2**, 723 (1970).
[44] J. Stephenson, Can. J. Phys. **47**, 2621 (1969).
[45] J. H. Barry, T. Tanaka, M. Khatun, and C. H. Munera, Phys. Rev. B **44**, 2595 (1991).